Analysis of an arbitrarily oriented crack in a finite piezoelectric plane via the hybrid extended displacement discontinuity-fundamental solution method

CuiYing Fan, MingHao Zhao, JiaPeng Wang & Ernian Pan

Computational Mechanics
Solids, Fluids, Structures, Fluid-Structure Interactions, Biomechanics, Micromechanics, Multiscale Mechanics, Materials, Constitutive Modeling, Nonlinear Mechanics, Aerodynamics

ISSN 0178-7675
Volume 51
Number 4

Comput Mech (2013) 51:567-580
DOI 10.1007/s00466-012-0754-2

Springer

Comput Mech (2013) 51:567–580
DOI 10.1007/s00466-012-0754-2

ORIGINAL PAPER

Analysis of an arbitrarily oriented crack in a finite piezoelectric plane via the hybrid extended displacement discontinuity-fundamental solution method

CuiYing Fan · MingHao Zhao · JiaPeng Wang · Ernian Pan

Received: 28 February 2012 / Accepted: 27 June 2012 / Published online: 11 July 2012

Abstract In this paper, we analyze an arbitrarily oriented crack in a finite two-dimensional piezoelectric medium with the polarization saturation model near the crack tip. We first derive the extended Green's functions corresponding to the extended point-displacement discontinuities of an arbitrarily oriented crack based on the Green's functions of the extended point forces and the Somigliana identity. Then, the extended field intensity factors and the local J-integral near the crack tip are expressed in terms of the extended displacement discontinuity on crack faces. Finally, the nonlinear hybrid extended displacement discontinuity-fundamental solution method is proposed to analyze an electrically nonlinear crack in a finite piezoelectric medium. Numerical examples are carried out for both linear and nonlinear fracture models of the crack under electrically impermeable boundary conditions. The influence of the crack orientation and geometric size on the fracture behaviors of the crack is investigated.

Keywords Piezoelectric medium · Arbitrarily oriented crack · NLHEDD-FS method · PS model · Extended field intensity factor · Local J-integral

1 Introduction

Along with the wide use of piezoelectric ceramics in smart structures, research in fracture of these materials has been receiving a great deal of attention [1–4]. Previous studies were mostly limited to cracks lying in the plane of isotropy in transversely isotropic piezoelectric media. In reality, however, the cracks distributed in the structure could be in any orientation. As such, the corresponding problem where a crack is oriented arbitrarily is of theoretical significance and application value.

Research of an arbitrarily oriented crack in elastic media can be traced back to 1974 when the problem of a crack arbitrarily oriented with respect to the interface of a bimaterial plane was solved by Erdogan and Aksogan [5]. Later, Erdogan and Arin [6] solved the problem of a crack arbitrarily oriented with respect to the interface of a strip and half-plane materials. For piezoelectric media, Tian and Chau [7] studied an arbitrarily oriented crack near the interface of piezoelectric bimaterials, and the stress intensity factors and the electric displacement intensity factor at the crack tips were evaluated by the dislocation density function method. Using a dielectric crack model, Wang et al. [8] studied the effects of the crack orientation and the applied loads upon the fracture behavior of the crack in piezoelectric materials. Chue and Weng [9] found that a negative electric field impeded the crack growth whereas a positive electric field enhanced it and that the driving force and the crack propagation angle were significantly influenced by the polarization direction. Ang and Athanasius [10] studied the dynamic problem of multiple arbitrarily oriented planar cracks in a piezoelectric space under a transient load. The fracture behavior of a crack in a piezoelectric medium could be nonlinear, yet, there are only very few reports on this issue.

As is well known, the extension of the current fundamental fracture concepts or criteria in pure elasticity to piezoelectricity is not straightforward since the coupling between the mechanical and electric fields is complicated [1,3]. Gao et al. [11] extended the classical Dugdale model [12] to a

C. Fan · M. Zhao (✉) · E. Pan
The School of Mechanical Engineering, Zhengzhou University, No. 100 Science Road, Zhengzhou 450001, Henan, People's Republic of China
e-mail: memhzhao@zzu.edu.cn; memhzhao@sina.com

M. Zhao · J. Wang
Department of Engineering Mechanics, Zhengzhou University, Zhengzhou 450001, Henan, People's Republic of China

strip polarization saturation (PS) model in piezoelectricity by assuming that the electric displacement is constant in a strip adjacent to a crack tip. Zhang et al. [13] proposed a strip dielectric breakdown (DB) model assuming that the electric field strength be constant in a strip adjacent to a crack tip. It is found that the DB model gives the same results as the PS model in predicting the effect of an applied electric field on the fracture of piezoelectric media [13]. Later, piezoelectric fracture analyses based on the PS and DB models were also conducted by Ru and Mao [14], Beom et al. [15], Gao et al. [16], Loboda et al. [17], among others.

Analytical solutions are usually difficult to obtain, especially for the nonlinear fracture problem in a finite domain. Recently, in order to study the effect of the electric boundary condition on the field quantities, Fan et al. [18] and Zhao et al. [19] developed a numerical method, the nonlinear hybrid extended displacement discontinuity-fundamental solution (NLHEDD-FS) method, where both the PS and DB models can be considered. This method was also used to study the linear and nonlinear fracture of magnetoelectroelastic media [20,21]. In this method, the extended point-force fundamental solutions and the extended Crouch fundamental solutions with extended displacement discontinuities play an important role. Therefore, in order to study an arbitrarily oriented crack in a finite piezoelectric plane, we first, in this paper, derive the extended point-displacement discontinuity fundamental solution for an arbitrarily oriented crack by using the Green's functions of the extended point forces and the Somigliana identity. Then the extended Crouch fundamental solutions are obtained. Furthermore, the extended field intensity factors near the crack tip and local J-integral are expressed in terms of the extended displacement discontinuity on crack faces. Finally the NLHEDD-FS method with an iterative approach is developed to study the piezoelectric fracture behavior of an arbitrarily oriented crack.

2 Basic equations

For a two-dimensional (2D) piezoelectric medium in the coordinate system oyz, in the absence of the body force and electric charge, the equilibrium equations, kinematic equations and constitutive equations are given by

$$\sigma_{ij,j} = 0, \quad D_{i,i} = 0, \tag{1}$$

$$\varepsilon_{ij} = \frac{1}{2}\left(u_{i,j} + u_{j,i}\right), \quad E_i = -\varphi_{,i}, \tag{2}$$

$$\sigma_{ij} = C_{ijkl}\varepsilon_{kl} - e_{kij}E_k, \tag{3a}$$

$$D_i = e_{ikl}\varepsilon_{kl} + \kappa_{ik}E_k, \tag{3b}$$

where $\sigma_{ij}, \varepsilon_{ij}, D_i$ and E_i denote the stress, strain, electric displacement and electric field strength, respectively; $u_i((u_1, u_2) = (v, w))$ and φ are the elastic displacements and electric potential, respectively; and $C_{ijkl}(\equiv c_{ij}), e_{ijk}(\equiv e_{ij})$ and κ_{ij} stand for the elastic, piezoelectric and the dielectric constants, respectively.

3 Boundary integral expressions

We assume that there is a straight line crack S lying in the oyz plane, as shown in Fig. 1. The poling direction of the piezoelectric material is along the z-direction. The crack is oriented arbitrarily with respect to the y-axis by angle β. The upper and lower faces of the crack S are denoted by S^+ and S^-, respectively. The outer normal vectors of S^+ and $S^-$are respectively given by

$$\{n_i\}^+ = \{\sin\beta, -\cos\beta\}, \quad \{n_i\}^- = \{-\sin\beta, \cos\beta\}. \tag{4}$$

Making use of the extended point-force Green's functions [22] and the Somigliana identity for piezoelectric media, the elastic displacements and the electric potential at any point (y, z) can be expressed by the following integrals

$$u_i(y,z) = -\int_{S^+} \left[P_{ij}^{\mathrm{F}} \left\|u_j\right\| + \Omega_i^{\mathrm{F}} \left\|\varphi\right\|\right] dS,$$

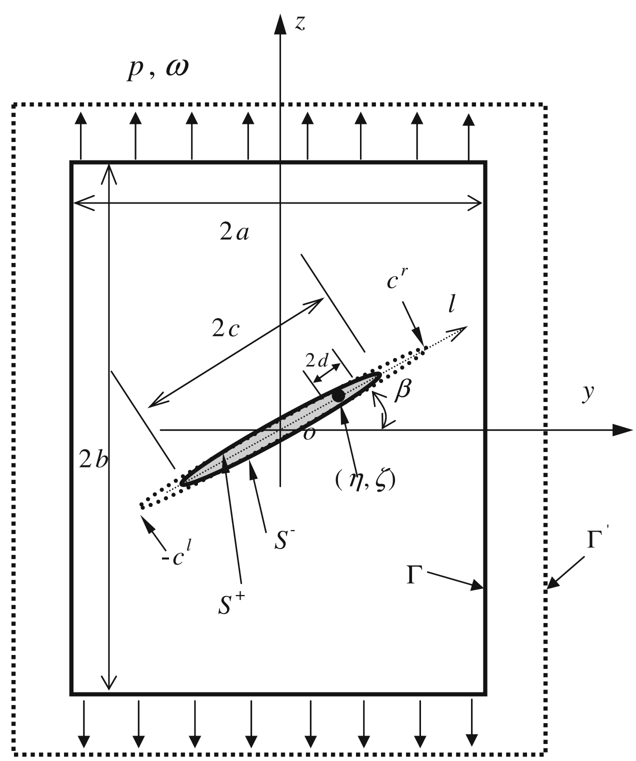

Fig. 1 An arbitrarily oriented straight line crack S in a piezoelectric rectangle and one of the elements along it. While $2c$ is the crack length, $2d$ represents one of the elements along the crack surface, S^+ and S^- denote the upper and lower faces of crack S

$$-\varphi(y,z) = -\int_{S^+} \left[P_j^{\mathrm{D}} \left\| u_j \right\| + \Omega^{\mathrm{D}} \left\| \varphi \right\| \right] dS, \tag{5}$$

where P_{ij}^{F} and Ω_i^{F}, are, respectively, the induced tractions and electric displacements on the crack surfaces when a unit point force is applied in the ith direction; P_j^{D} and Ω^{D} are those corresponding to a unit point electric charge. In Eq. (5), $\left\| u_j \right\|$ and $\left\| \varphi \right\|$ denote, respectively, the elastic displacement and electric potential discontinuities across the crack face, defined as

$$\begin{aligned} \left\| u_i \right\| &= u_i(S^+) - u_i(S^-), \\ \left\| \varphi \right\| &= \varphi(S^+) - \varphi(S^-), \end{aligned} \tag{6}$$

which are called the extended displacement discontinuities.

Inserting the extended point-force Green's functions [22] into Eq. (5) yields the following explicit expressions for the elastic displacement and electric potential

$$\begin{aligned} v = \int_{S^+} \Bigg\{ & \left\| v \right\| \left(\sum_{i=1}^{3} \omega_{i1} D_i \frac{-2(\varsigma_i - z_i)\cos\beta}{(\eta - y)^2 + (\varsigma_i - z_i)^2} + (c_{11} - c_{12} - \xi_i) D_i \frac{2(\eta - y)\sin\beta}{(\eta - y)^2 + (\varsigma_i - z_i)^2} \right) \\ & + \left\| w \right\| \left(\sum_{i=1}^{3} \vartheta_{i1} D_i \frac{2(\eta - y)\cos\beta}{(\eta - y)^2 + (\varsigma_i - z_i)^2} + \omega_{i1} D_i \frac{2(\varsigma_i - z_i)\sin\beta}{(\eta - y)^2 + (\varsigma_i - z_i)^2} \right) \\ & + \left\| \varphi \right\| \left(\sum_{i=1}^{3} \vartheta_{i2} D_i \frac{2(\eta - y)\cos\beta}{(\eta - y)^2 + (\varsigma_i - z_i)^2} + \omega_{i2} D_i \frac{2(\varsigma_i - z_i)\sin\beta}{(\eta - y)^2 + (\varsigma_i - z_i)^2} \right) \Bigg\} dS(\eta, \varsigma_i), \end{aligned} \tag{7a}$$

$$\begin{aligned} w = \int_{S^+} \Bigg\{ & \left\| v \right\| \left(\sum_{i=1}^{3} (c_{11} - c_{12} - \xi_i) \times A_i \frac{2(\varsigma_i - z_i)\sin\beta}{(\eta - y)^2 + (\varsigma_i - z_i)^2} + \omega_{i1} A_i \frac{2(\eta - y)\cos\beta}{(\eta - y)^2 + (\varsigma_i - z_i)^2} \right) \\ & + \left\| w \right\| \left(\sum_{i=1}^{3} \vartheta_{i1} A_i \frac{2(\varsigma_i - z_i)\cos\beta}{(\eta - y)^2 + (\varsigma_i - z_i)^2} + \omega_{i1} A_i \frac{-2(\eta - y)\sin\beta}{(\eta - y)^2 + (\varsigma_i - z_i)^2} \right) \\ & + \left\| \varphi \right\| \left(\sum_{i=1}^{3} \vartheta_{i2} A_i \frac{2(\varsigma_i - z_i)\cos\beta}{(\eta - y)^2 + (\varsigma_i - z_i)^2} + \omega_{i2} A_i \frac{-2(\eta - y)\sin\beta}{(\eta - y)^2 + (\varsigma_i - z_i)^2} \right) \Bigg\} dS(\eta, \varsigma_i), \end{aligned} \tag{7b}$$

$$\begin{aligned} -\varphi = \int_{S^+} \Bigg\{ & \left\| v \right\| \left(\sum_{i=1}^{3} (c_{11} - c_{12} - \xi_i) \times B_i \frac{2(\varsigma_i - z_i)\sin\beta}{(\eta - y)^2 + (\varsigma_i - z_i)^2} + \omega_{i1} B_i \frac{2(\eta - y)\cos\beta}{(\eta - y)^2 + (\varsigma_i - z_i)^2} \right) \\ & + \left\| w \right\| \left(\sum_{i=1}^{3} \vartheta_{i1} B_i \frac{2(\varsigma_i - z_i)\cos\beta}{(\eta - y)^2 + (\varsigma_i - z_i)^2} + \omega_{i1} B_i \frac{-2(\eta - y)\sin\beta}{(\eta - y)^2 + (\varsigma_i - z_i)^2} \right) \\ & + \left\| \varphi \right\| \left(\sum_{i=1}^{3} \vartheta_{i2} B_i \frac{2(\varsigma_i - z_i)\cos\beta}{(\eta - y)^2 + (\varsigma_i - z_i)^2} + \omega_{i2} B_i \frac{-2(\eta - y)\sin\beta}{(\eta - y)^2 + (\varsigma_i - z_i)^2} \right) \Bigg\} dS(\eta, \varsigma_i). \end{aligned} \tag{7c}$$

Equation (7) indicates that the extended displacements at any point (y, z) can be expressed in terms of the extended displacement discontinuities across the surface of the crack, where

$$z_i = s_i z, \quad \varsigma_i = s_i \varsigma, \quad (i = 1, 2, 3, 4), \tag{8}$$

and s_i are the roots of the material characteristic equation, whilst ω_{ij}, ξ_i, A_i, B_i and D_i in Eq. (7) are material-related constants given in [18]. It is noted that constants D_i are different to the electric displacements defined in Eqs. (1) and (3b).

4 Green's functions and the extended Crouch fundamental solution for extended displacement discontinuities

We assume that the length of the straight line crack S is 2c centered at the origin of the coordinate system, as shown in Fig. 1. When the size of the crack approaches zero, the Green's functions or the fundamental solutions corresponding to a unit extended point displacement discontinuity is obtained. Therefore, such displacement discontinuity Green's functions should satisfy the governing equations of piezoelectric media subjected to the following conditions, respectively

$$\lim_{a \to 0} \int_S \{\left\| v \right\|, \left\| w \right\|, \left\| \varphi \right\|\} dS = \{1, 0, 0\}, \tag{9a}$$

$$\lim_{a \to 0} \int_S \{\left\| v \right\|, \left\| w \right\|, \left\| \varphi \right\|\} dS = \{0, 1, 0\}, \tag{9b}$$

$$\lim_{a \to 0} \int_S \{\left\| v \right\|, \left\| w \right\|, \left\| \varphi \right\|\} dS = \{0, 0, 1\}. \tag{9c}$$

Making use of the method in deriving the extended point-displacement discontinuity Green's functions [23], we obtain the extended point-displacement discontinuity Green's functions satisfying Eq. (9a)

$$v = 2\sum_{i=1}^{3}\left(\omega_{i1}D_i\frac{z_i\cos\beta}{y^2+z_i^2} - (c_{11}-c_{12}-\xi_i)D_i\frac{y\sin\beta}{y^2+z_i^2}\right), \quad (10a)$$

$$w = -2\sum_{i=1}^{3}\left(\omega_{i1}A_i\frac{y\cos\beta}{y^2+z_i^2} + (c_{11}-c_{12}-\xi_i)A_i\frac{z_i\sin\beta}{y^2+z_i^2}\right), \quad (10b)$$

$$\varphi = 2\sum_{i=1}^{3}\left(\omega_{i1}B_i\frac{y\cos\beta}{y^2+z_i^2} + (c_{11}-c_{12}-\xi_i)B_i\frac{z_i\sin\beta}{y^2+z_i^2}\right). \quad (10c)$$

Similarly, the extended point-displacement discontinuity Green's functions satisfying Eq. (9b) can be expressed by

$$v = -2\sum_{i=1}^{3}\left(\vartheta_{i1}D_i\frac{y\cos\beta}{y^2+z_i^2} + \omega_{i1}D_i\frac{z_i\sin\beta}{y^2+z_i^2}\right), \quad (11a)$$

$$w = -2\sum_{i=1}^{3}\left(\vartheta_{i1}A_i\frac{z_i\cos\beta}{y^2+z_i^2} - \omega_{i1}A_i\frac{y\sin\beta}{y^2+z_i^2}\right), \quad (11b)$$

$$\varphi = 2\sum_{i=1}^{3}\left(\vartheta_{i1}B_i\frac{z_i\cos\beta}{y^2+z_i^2} - \omega_{i1}B_i\frac{y\sin\beta}{y^2+z_i^2}\right). \quad (11c)$$

Green's functions for unit point electric potential discontinuity satisfying Eq. (9c) can be obtained simply by replacing the material related constant ϑ_{i1} in Eq. (11) by ϑ_{i2}. Then substituting Eqs. (10) and (11) into the constitutive equation i.e., Eq. (3), yields the corresponding stress and electric displacement fields.

We consider a straight line element of length $2d$, inclined with respect to the y-axis by the angle β, centered at point (η, ς), as shown in Fig. 1. Along the element, we apply uniformly distributed displacement discontinuities $\|v^e\|$ in y-direction, $\|w^e\|$ in z-direction and the electric potential discontinuity $\|\varphi^e\|$. Integrating the extended point-displacement discontinuity Green's functions along the element gives the extended Crouch fundamental solutions

$$\begin{aligned}\sigma_{yy}^e = 2\sum_{i=1}^{3}\Big\{\Big[&\cos\beta\,\|v^e\|\,L_{fyy21}^i + \sin\beta\,\|w^e\|\,L_{fyy31}\\ &+ \sin\beta\,\|\varphi^e\|\,L_{fyy41}^i\Big]G_1\\ &+\Big[\sin\beta\,\|v^e\|\,L_{fyy22}^i + \cos\beta\,\|w^e\|\,L_{fyy32}^i\\ &+ \cos\beta\,\|\varphi^e\|\,L_{fyy42}^i\Big]G_2\Big\},\end{aligned} \quad (12a)$$

$$\begin{aligned}\sigma_{yz}^e = 2\sum_{i=1}^{3}\Big\{\Big[&\sin\beta\,\|v^e\|\,L_{fy21}^i + \cos\beta\,\|w^e\|\,L_{fy31}^i\\ &+ \cos\beta\,\|\varphi^e\|\,L_{fy41}^i\Big]G_1\\ &+\Big[\cos\beta\,\|v^e\|\,L_{fy22}^i + \sin\beta\,\|w^e\|\,L_{fy32}^i\\ &+ \sin\beta\,\|\varphi^e\|\,L_{fy42}^i\Big]G_2\Big\},\end{aligned} \quad (12b)$$

$$\begin{aligned}\sigma_{zz}^e = 2\sum_{i=1}^{3}\Big\{\Big[&\cos\beta\,\|v^e\|\,L_{f21}^i + \sin\beta\,\|w^e\|\,L_{f31}^i\\ &+ \sin\beta\,\|\varphi^e\|\,L_{f41}^i\Big]G_1\\ &+\Big[\sin\beta\,\|v^e\|\,L_{f22}^i + \cos\beta\,\|w^e\|\,L_{f32}^i\\ &+ \cos\beta\,\|\varphi^e\|\,L_{f42}^i\Big]G_2\Big\},\end{aligned} \quad (12c)$$

$$\begin{aligned}D_y^e = 2\sum_{i=1}^{3}\Big\{\Big[&\sin\beta\,\|v^e\|\,L_{dy21}^i + \cos\beta\,\|w^e\|\,L_{dy31}^i\\ &+ \cos\beta\,\|\varphi^e\|\,L_{dy41}^i\Big]G_1\\ &+\Big[\cos\beta\,\|v^e\|\,L_{dy22}^i + \sin\beta\,\|w^e\|\,L_{dy32}^i\\ &+ \sin\beta\,\|\varphi^e\|\,L_{dy42}^i\Big]G_2\Big\},\end{aligned} \quad (12d)$$

$$\begin{aligned}D_z^e = 2\sum_{i=1}^{3}\Big\{\Big[&\cos\beta\,\|v^e\|\,L_{d21}^i + \sin\beta\,\|w^e\|\,L_{d31}^i\\ &+ \sin\beta\,\|\varphi^e\|\,L_{d41}^i\Big]G_1\\ &+\Big[\sin\beta\,\|v^e\|\,L_{d22}^i + \cos\beta\,\|w^e\|\,L_{d32}^i\\ &+ \cos\beta\,\|\varphi^e\|\,L_{d42}^i\Big]G_2\Big\},\end{aligned} \quad (12e)$$

where L_{ijk}^i are the material-related constants given in Appendix A, and

$$\begin{aligned}G_1 = &-\frac{z_i\cos\beta + s_i(y-2d\cos\beta)\sin\beta}{\left[-1+\left(1-s_i^2\right)\sin^2\beta\right]\left[d^2\left(1-\sin^2\beta\left(1-s_i^2\right)\right)+y^2+z_i^2-2d\left(y\cos\beta+s_iz_i\sin\beta\right)\right]}\\ &+\frac{z_i\cos\beta + s_i\left(y+2c\cos\beta\right)\sin\beta}{\left[-1+\left(1-s_i^2\right)\sin^2\beta\right]\left[d^2\left(1-\sin^2\beta\left(1-s_i^2\right)\right)+y^2+z_i^2+2d\left(y\cos\beta+s_iz_i\sin\beta\right)\right]},\end{aligned} \quad (13a)$$

$$\begin{aligned}G_2 = &\frac{d\left[1-\sin^2\beta\left(1+s_i^2\right)\right]-y\cos\beta+s_iz_i\sin\beta}{\left[-1+\left(1-s_i^2\right)\sin^2\beta\right]\left[d^2\left(1-\sin^2\beta\left(1-s_i^2\right)\right)+y^2+z_i^2-2d\left(y\cos\beta+s_iz_i\sin\beta\right)\right]}\\ &-\frac{-d\left[1-\sin^2\beta\left(1+s_i^2\right)\right]-y\cos\beta+s_iz_i\sin\beta}{\left[-1+\left(1-s_i^2\right)\sin^2\beta\right]\left[d^2\left(1-\sin^2\beta\left(1-s_i^2\right)\right)+y^2+z_i^2+2d\left(y\cos\beta+s_iz_i\sin\beta\right)\right]}.\end{aligned} \quad (13b)$$

5 Extended field intensity factors and local J-integral

Based on the extended displacement discontinuity Green's functions in Sect. 4, the extended stresses at any point (y, z) can be expressed in terms of the integral of the extended displacement discontinuity on the entire crack faces

$$\begin{aligned}\sigma_{yy}(y,z) &= 2\sum_{i=1}^{3}\int_S \Big\{\Big[\cos\beta\,\|v\|\,L^i_{fyy21} + \sin\beta\,\|w\|\,L^i_{fyy31} + \sin\beta\,\|\varphi\|\,L^i_{fyy41}\Big]V_1 \\ &\quad + \Big[\sin\beta\,\|v\|\,L^i_{fyy22} + \cos\beta\,\|w\|\,L^i_{fyy32} + \cos\beta\,\|\varphi\|\,L^i_{fyy42}\Big]V_2\Big\}\,dS(\eta,\varsigma_i), \quad (14a)\end{aligned}$$

$$\begin{aligned}\sigma_{yz}(y,z) &= 2\sum_{i=1}^{3}\int_S \Big\{\Big[\sin\beta\,\|v\|\,L^i_{fy21} + \cos\beta\,\|w\|\,L^i_{fy31} + \cos\beta\,\|\varphi\|\,L^i_{fy41}\Big]V_1 \\ &\quad + \Big[\cos\beta\,\|v\|\,L^i_{fy22} + \sin\beta\,\|w\|\,L^i_{fy32} + \sin\beta\,\|\varphi\|\,L^i_{fy42}\Big]V_2\Big\}\,dS(\eta,\varsigma_i), \quad (14b)\end{aligned}$$

$$\begin{aligned}\sigma_{zz}(y,z) &= 2\sum_{i=1}^{3}\int_S \Big\{\Big[\cos\beta\,\|v\|\,L^i_{f21} + \sin\beta\,\|w\|\,L^i_{f31} + \sin\beta\,\|\varphi\|\,L^i_{f41}\Big]V_1 \\ &\quad + \Big[\sin\beta\,\|v\|\,L^i_{f22} + \cos\beta\,\|w\|\,L^i_{f32} + \cos\beta\,\|\varphi\|\,L^i_{f42}\Big]V_2\Big\}\,dS(\eta,\varsigma_i), \quad (14c)\end{aligned}$$

$$\begin{aligned}D_y(y,z) &= 2\sum_{i=1}^{3}\int_S \Big\{\Big[\sin\beta\,\|v\|\,L^i_{dy21} + \cos\beta\,\|w\|\,L^i_{dy31} + \cos\beta\,\|\varphi\|\,L^i_{dy41}\Big]V_1 \\ &\quad + \Big[\cos\beta\,\|v\|\,L^i_{dy22} + \sin\beta\,\|w\|\,L^i_{dy32} + \sin\beta\,\|\varphi\|\,L^i_{dy42}\Big]V_2\Big\}\,dS(\eta,\varsigma_i), \quad (14d)\end{aligned}$$

$$\begin{aligned}D_z(y,z) &= 2\sum_{i=1}^{3}\int_S \Big\{\Big[\cos\beta\,\|v\|\,L^i_{d21} + \sin\beta\,\|w\|\,L^i_{d31} + \sin\beta\,\|\varphi\|\,L^i_{d41}\Big]V_1 \\ &\quad + \Big[\sin\beta\,\|v\|\,L^i_{d22} + \cos\beta\,\|w\|\,L^i_{d32} + \cos\beta\,\|\varphi\|\,L^i_{d42}\Big]V_2\Big\}\,dS(\eta,\varsigma_i), \quad (14e)\end{aligned}$$

where

$$V_1 = \frac{2(y-\eta)(z_i-\varsigma_i)}{[(y-\eta)^2+(z_i-\varsigma_i)^2]^2},\quad V_2 = \frac{(y-\eta)^2-(z_i-\varsigma_i)^2}{[(y-\eta)^2+(z_i-\varsigma_i)^2]^2}. \quad (15)$$

It has been proven that the extended stress field has the classical singularity of order $1/\sqrt{r}$ near the crack tip in the 2D piezoelectric media. Thus, the extended displacement discontinuities at the neighborhood of the right crack tip (y_c, z_c) on the crack line can be expressed

$$\|v\| = A_y\sqrt{\delta},\qquad \|w\| = A_z\sqrt{\delta},\qquad \|\varphi\| = A_\varphi\sqrt{\delta}, \quad (16)$$

where δ is the distance from the crack tip and the coefficients A_y, A_z and A_φ are constants to be determined.

In the local polar coordinate system (r, θ) with the origin coinciding with the right crack tip, a point near the crack tip can be expressed by

$$y - y_c = r\cos\theta,\quad z_i - s_i z_c = s_i r\sin\theta,\quad r \ll 1. \quad (17)$$

Substituting Eqs. (16) and (17) into Eq. (14) introducing function f_{1i} and f_{2i} for the following integrals

$$2\int_{-\infty}^{0}\frac{2(\cos\theta-\hat{g}\cos\beta)(s_i\sin\theta-s_i\hat{g}\sin\beta)}{[(\cos\theta-\hat{g}\cos\beta)^2+(s_i\sin\theta-s_i\hat{g}\sin\beta)^2]^2}\times(-\hat{g})^{\frac{1}{2}}d\hat{g} = f_{1i}(\beta,\theta), \quad (18a)$$

$$2\int_{-\infty}^{0}\frac{(\cos\theta-\hat{g}\cos\beta)^2-(s_i\sin\theta-s_i\hat{g}\sin\beta)^2}{[(\cos\theta-\hat{g}\cos\beta)^2+(s_i\sin\theta-s_i\hat{g}\sin\beta)^2]^2}\times(-\hat{g})^{\frac{1}{2}}d\hat{g} = f_{2i}(\beta,\theta), \quad (18b)$$

the extended stresses at an arbitrary point near the crack tip can be expressed by

$$\begin{aligned}\sigma_{yy} &= \frac{1}{\sqrt{r}}\sum_{i=1}^{3}\Big\{\Big[\cos\beta A_y L^i_{fyy21} + \sin\beta A_z L^i_{fyy31} + \sin\beta A_\varphi L^i_{fyy41}\Big]f_{1i}(\beta,\theta) \\ &\quad + \Big[\sin\beta A_y L^i_{fyy22} + \cos\beta A_z L^i_{fyy32} + \cos\beta A_\varphi L^i_{fyy42}\Big]f_{2i}(\beta,\theta)\Big\}, \quad (19a)\end{aligned}$$

$$\begin{aligned}\sigma_{yz} &= \frac{1}{\sqrt{r}}\sum_{i=1}^{3}\Big\{\Big[\sin\beta L^i_{fy21}A_y + \cos\beta L^i_{fy31}A_z + \cos\beta L^i_{fy41}A_\varphi\Big]f_{1i}(\beta,\theta) \\ &\quad + \Big[\cos\beta L^i_{fy22}A_y + \sin\beta L^i_{fy32}A_z + \sin\beta L^i_{fy42}A_\varphi\Big]f_{2i}(\beta,\theta)\Big\}, \quad (19b)\end{aligned}$$

$$\sigma_{zz} = \frac{1}{\sqrt{r}} \sum_{i=1}^{3} \left\{ \left[\cos\beta L^i_{f21} A_y + \sin\beta L^i_{f31} A_w + \sin\beta L^i_{f41} A_\varphi \right] f_{1i}(\beta,\theta) + \left[\sin\beta L^i_{f22} A_y + \cos\beta L^i_{f32} A_w + \cos\beta L^i_{f42} A_\varphi \right] f_{2i}(\beta,\theta) \right\}, \tag{19c}$$

$$D_y = \frac{1}{\sqrt{r}} \sum_{i=1}^{3} \left\{ \left[\sin\beta L^i_{dy21} A_y + \cos\beta L^i_{dy31} A_z + \cos\beta L^i_{dy41} A_\varphi \right] f_{1i}(\beta,\theta) + \left[\cos\beta L^i_{dy22} A_y + \sin\beta L^i_{dy32} A_z + \sin\beta L^i_{dy42} A_\varphi \right] f_{2i}(\beta,\theta) \right\}, \tag{19d}$$

$$D_z = \frac{1}{\sqrt{r}} \sum_{i=1}^{3} \left\{ \left[\cos\beta L^i_{d21} A_y + \sin\beta L^i_{d31} A_z + \sin\beta L^i_{d41} A_\varphi \right] f_{1i}(\beta,\theta) + \left[\sin\beta L^i_{d22} A_y + \cos\beta L^i_{d32} A_z + \cos\beta L^i_{d42} A_\varphi \right] f_{2i}(\beta,\theta) \right\}. \tag{19e}$$

When $\theta = \beta$, we define the extended intensity factors

$$\begin{aligned} K_{\mathrm{I}}^F &= \lim_{r\to 0} \sqrt{2\pi r}\,\sigma'_{\mathrm{I}}(r,0), \\ K_{\mathrm{II}}^F &= \lim_{r\to 0} \sqrt{2\pi r}\,\sigma'_{\mathrm{II}}(r,0), \\ K_{\mathrm{I}}^D &= \lim_{r\to 0} \sqrt{2\pi r}\,D'_{\mathrm{I}}(r,0). \end{aligned} \tag{20}$$

where σ'_{I}, σ'_{II} and D'_{I} stand for the extended stresses along the crack line

$$\begin{aligned} \sigma'_{\mathrm{I}} &= \sigma_{yy}\sin^2\beta + \sigma_{zz}\cos^2\beta - 2\sigma_{yz}\sin\beta\cos\beta, \\ \sigma'_{\mathrm{II}} &= (\sigma_{zz} - \sigma_{yy})\sin\beta\cos\beta + \sigma_{yz}\cos 2\beta, \\ D'_{\mathrm{I}} &= -D_y\sin\beta + D_z\cos\beta. \end{aligned} \tag{21}$$

Inserting Eqs. (19) and (21) into Eq. (20) gives

$$K_{\mathrm{I}} = \lim_{r\to 0} \frac{\sqrt{2\pi}}{\sqrt{r}} \left[k_{11}\|v\| + k_{12}\|w\| + k_{13}\|\varphi\| \right], \tag{22a}$$

$$K_{\mathrm{II}} = \lim_{r\to 0} \frac{\sqrt{2\pi}}{\sqrt{r}} [k_{21}\|v\| + k_{22}\|w\| + k_{23}\|\varphi\|], \tag{22b}$$

$$K_{\mathrm{D}} = \lim_{r\to 0} \frac{\sqrt{2\pi}}{\sqrt{r}} [k_{31}\|v\| + k_{32}\|w\| + k_{33}\|\varphi\|], \tag{22c}$$

where

$$k_{11} = \sum_{i=1}^{3} \left\{ \left[(\sin\beta)^2 \cos\beta L^i_{fyy21} + \cos^3\beta L^i_{f21} - \sin 2\beta \sin\beta L^i_{fy21} \right] f_{1i}(\beta,\theta) + \left[(\sin\beta)^3 L^i_{fyy22} + \cos^2\beta \sin\beta L^i_{f22} - \sin 2\beta \cos\beta L^i_{fy22} \right] f_{2i}(\beta,\theta) \right\}, \tag{23a}$$

$$k_{12} = \sum_{i=1}^{3} \left\{ \left[(\sin\beta)^3 L^i_{fyy31} + \cos^2\beta \sin\beta L^i_{f31} - \sin 2\beta \cos\beta L^i_{fy31} \right] f_{1i}(\beta,\theta) + \left[(\sin\beta)^2 \cos\beta L^i_{fyy32} + \cos^3\beta L^i_{f32} - \sin 2\beta \sin\beta L^i_{fy32} \right] f_{2i}(\beta,\theta) \right\}, \tag{23b}$$

$$k_{13} = \sum_{i=1}^{3} \left\{ \left[(\sin\beta)^3 L^i_{fyy41} + \cos^2\beta \sin\beta L^i_{f41} - \sin 2\beta \cos\beta L^i_{fy41} \right] f_{1i}(\beta,\theta) + \left[(\sin\beta)^2 \cos\beta L^i_{fyy42} + \cos^3\beta L^i_{f42} - \sin 2\beta \sin\beta L^i_{fy42} \right] f_{2i}(\beta,\theta) \right\}, \tag{23c}$$

$$k_{21} = \sum_{i=1}^{3} \left\{ \left[\sin\beta\cos^2\beta \left(L^i_{f21} - L^i_{fyy21} \right) + \cos 2\beta \sin\beta L^i_{fy21} \right] f_{1i}(\beta,\theta) + \left[\cos\beta\sin^2\beta \left(L^i_{f22} - L^i_{fyy22} \right) + \cos 2\beta \cos\beta L^i_{fy22} \right] f_{2i}(\beta,\theta) \right\}, \tag{23d}$$

$$k_{22} = \sum_{i=1}^{3} \left\{ \left[\cos\beta\sin^2\beta \left(L^i_{f31} - L^i_{fyy31} \right) + \cos 2\beta \cos\beta L^i_{fy31} \right] f_{1i}(\beta,\theta) + \left[\sin\beta\cos^2\beta \left(L^i_{f32} - L^i_{fyy32} \right) + \cos 2\beta \sin\beta L^i_{fy32} \right] f_{2i}(\beta,\theta) \right\}, \tag{23e}$$

$$k_{23} = \sum_{i=1}^{3} \left\{ \left[\cos\beta\sin^2\beta \left(L^i_{f41} - L^i_{fyy41} \right) + \cos 2\beta \cos\beta L^i_{fy41} \right] f_{1i}(\beta,\theta) + \left[\sin\beta\cos^2\beta (L^i_{f42} - L^i_{fyy42}) + \cos 2\beta \sin\beta L^i_{fy42} \right] f_{2i}(\beta,\theta) \right\}, \tag{23f}$$

$$k_{31} = \sum_{i=1}^{3} \left\{ \left[\cos^2\beta L^i_{d21} - \sin^2\beta L^i_{dy21} \right] f_{1i}(\beta,\theta) + \left[\cos\beta\sin\beta L^i_{d22} - \sin\beta\cos\beta L^i_{dy22} \right] f_{2i}(\beta,\theta) \right\}, \tag{23g}$$

$$k_{32}=\sum_{i=1}^{3}\left\{\left[\sin\beta\cos\beta L_{d31}^{i}-\sin\beta\cos\beta L_{dy31}^{i}\right]f_{1i}(\beta,\theta)+\left[\cos^{2}\beta L_{d32}^{i}-\sin^{2}\beta L_{dy32}^{i}\right]f_{2i}(\beta,\theta)\right\},\tag{23h}$$

$$k_{33}=\sum_{i=1}^{3}\left\{\left[\sin\beta\cos\beta L_{d41}^{i}-\sin\beta\cos\beta L_{dy41}^{i}\right]f_{1i}(\beta,\theta)+\left[\cos^{2}\beta L_{d42}^{i}-\sin^{2}\beta L_{dy42}^{i}\right]f_{2i}(\beta,\theta)\right\}.\tag{23i}$$

Once the extended displacement discontinuities on the crack faces are obtained, the intensity factors can be calculated using Eq. (22). With these, the local J-integral can also be obtained via

$$J=\mathbf{K}^{\mathrm{T}}\frac{\mathbf{H}}{4}\mathbf{K},\tag{24}$$

where the matrix $\mathbf{H}$ can be found in Zhang et al. [3] and

$$\mathbf{K}=\left(K_{\mathrm{II}}\ K_{\mathrm{I}}\ 0\ K_{\mathrm{D}}\right)^{\mathrm{T}}.\tag{25}$$

6 NLHEDD-FS method of a crack in a finite piezoelectric medium based on PS model

We consider a piezoelectric medium occupying a finite domain Ω enclosed by the outer boundary Γ in a rectangular coordinate system oyz as shown in Fig. 1. The polarization direction of the piezoelectric medium is along z-axis. A straight line crack S with length $2c$ is oriented arbitrarily with respect to the y-axis by an angle β. Similar to the PS model [11,18], the PS zone is a strip along the crack line, with $-c_{\mathrm{e}}^{l}$ and c_{e}^{r} denoting the strip electric yielding zones respectively at the left and right crack tips.

There are two kinds of boundary conditions on the outer boundary Γ: mechanical and electric boundary conditions. The mechanical boundary conditions can be expressed as

$$v=\bar{v},\ w=\bar{w},\quad \text{on } \Gamma_u,\tag{26a}$$

$$t_y\equiv\sigma_y n_y+\tau_{yz}n_z=\bar{t}_y,\quad t_z\equiv\tau_{yz}n_y+\sigma_z n_z=\bar{t}_z,\quad \text{on } \Gamma_t,\tag{26b}$$

where t_y and t_z are the tractions along the y- or z-directions respectively, with the overbar "-" denoting the prescribed value on the boundary, and n_i is the directional cosine of the outward normal vector on the boundary. The electric boundary conditions are

$$\varphi=\overline{\varphi},\quad \text{on } \Gamma_\varphi,\tag{27c}$$

$$\omega\equiv D_y n_y+D_z n_z=\bar{\omega},\quad \text{on } \Gamma_\omega,\tag{27d}$$

where $\bar{\omega}$ is the boundary value of the electric displacement.

There are also two kinds of boundary conditions on the crack face S in the PS model. For an electrically impermeable crack, the mechanical boundary conditions on crack faces are similar to those in Eq. (26b), whilst the electric boundary condition is

$$D_y n_y+D_z n_z=0.\tag{28}$$

In both the left- and right-hand electric yielding zones, the boundary conditions are given as

$$\begin{aligned}&v(S^+)=v(S^-),\quad w(S^+)=w(S^-),\\&D_y n_y+D_z n_z+\omega_s=0,\quad -c^l\le l\le -c,\ c\le l\le c^r,\end{aligned}\tag{29}$$

where superscripts "+" and "−" are the quantities on the upper and lower crack faces, respectively, ω_{s} is the electric displacement saturation, and l is the length coordinate of the crack.

6.1 NLHEDD-FS for the PS model

Based on the NLHEDD-FS method for piezoelectric media [18], we use N_1 collocation points on the outer boundary Γ, with the equal number of source points N_1 being located on the virtual boundary Γ', as schematically shown in Fig. 1. The unknown extended concentrated loads P_{ki} $(k=1,2,\ldots,N_1;\ i=1,2,3)$ are applied at the kth source point, where P_{k1} and P_{k2} are the mechanical loads in y- and z-directions respectively, and P_{k3} is the electric point charge. The crack surface S is divided into N_2 constant elements, and the unknown extended displacement discontinuities $\|u_{kj}\|\equiv u_{kj}^{+}-u_{kj}^{-}$ $(k=1,2,\ldots,N_2;\ j=1,2,3)$ are assumed to be uniform on each element, where $\|\cdot\|$ denotes the discontinuity of the extended displacement across the crack. The left and right electric yielding zones are discretized, respectively, into N_3^l and N_3^r constant elements ($N_3=N_3^l+N_3^r$), with the unknown electric potential discontinuity $\|\varphi_k\|$ $(k=1,2,\ldots,N_3)$ on each element.

Using the extended point-force fundamental solutions and the extended Crouch fundamental solutions or constant element fundamental solutions in Sect. 4, and the method of superposition, we can express the extended displacement and stress fields at any field point $\boldsymbol{X}(\equiv(y,z))$ around an impermeable crack in the finite domain due to given mechanical and electric loadings as

$$u_i(\boldsymbol{X})=\sum_{k=1}^{N_1}\sum_{j=1}^{3}u_{ij}^{*}(\boldsymbol{X},\boldsymbol{X}_{\mathrm{P}})P_{kj}+\sum_{k=1}^{N_2}\sum_{j=1}^{3}u_{kj}^{\mathrm{c}}(\boldsymbol{X},\boldsymbol{X}_{\mathrm{S}})\left\|u_{kj}\right\|$$

$$+\sum_{k=1}^{N_3} u_{i3}^{\mathrm{c}}(\boldsymbol{X}, \boldsymbol{X}_{\mathrm{D}})\,\|\varphi_k\| \quad (i=1,\,2,\,3), \tag{30a}$$

$$\sigma_i(\boldsymbol{X}) = \sum_{k=1}^{N_1}\sum_{j=1}^{3} \sigma_{ij}^{*}(\boldsymbol{X}, \boldsymbol{X}_{\mathrm{P}}) P_{kj} + \sum_{k=1}^{N_2}\sum_{j=1}^{3} \sigma_{ij}^{\mathrm{c}}(\boldsymbol{X}, \boldsymbol{X}_{\mathrm{S}})\,\|u_{kj}\| + \sum_{k=1}^{N_3} \sigma_{i3}^{\mathrm{c}}(\boldsymbol{X}, \boldsymbol{X}_{D})\,\|\varphi_k\| \quad (i=1,2,3,4,5), \tag{30b}$$

where σ_1, σ_2, σ_3, σ_4 and σ_5 are the extended stresses σ_{yy}, σ_{zz}, σ_{yz}, D_y and D_z respectively; u_3 is the electric potential φ; u_{ij}^{*} and σ_{ij}^{*} are the above-mentioned fundamental solutions corresponding to the extended point forces, and u_{ij}^{c} and σ_{ij}^{c} are the extended Crouch fundamental solutions derived above; X_{P}, X_{S} and X_{D} denote, respectively, the source points outside the domain, on the crack and in the electric yielding zone (again each has two coordinates (y, z)).

Letting Eq. (30) satisfy the given boundary conditions at the collocation points on the boundary Γ and on the crack and in the yielding zones, one can obtain $3(N_1+N_2)+N_3$ linear algebraic equations for the unknown extended loads P_{ki} and the unknown extended discontinuity displacements $\|u_{kj}\|$. Solving these $3(N_1+N_2)+N_3$ equations determines the unknown quantities.

Furthermore, by fitting the calculated extended displacement discontinuity using the corresponding values at the $(N_{\mathrm{c}}-1)$th, N_{c}th and $(N_{\mathrm{c}}+1)$th elements from the crack tip, one obtains the asymptotic behavior of the extended displacement discontinuity near the crack tip

$$\begin{aligned} \|v\| &= \eta_{11} r^{1/2} + \eta_{12} r + \eta_{13} r^{3/2}, \\ \|w\| &= \eta_{21} r^{1/2} + \eta_{22} r + \eta_{23} r^{3/2}, \\ \|\varphi\| &= \eta_{30} + \eta_{31} r^{1/2} + \eta_{32} r + \eta_{33} r^{3/2}, \end{aligned} \tag{31}$$

where r is the relative distance of the point on the crack faces from the crack tip, η_{ij} fitting coefficients, and η_{30} represents the effect of the electric potential discontinuity in the electric yielding zone. Finally, the extended stress intensity factors and local J-integral can be calculated based on Eqs. (22) and (24).

6.2 Iterative approach for determining the electric yielding zone

In the method presented above, the size of the electric yielding zone is unknown, albeit related to the applied loadings and geometry of the finite piezoelectric medium. To determine the electric yielding zone, the following supplementary conditions on the electric displacement intensity factor must be used

$$K_{\mathrm{Ds}}^{r} = \lim_{l \to c^r} \sqrt{2\pi(l - c^r)}\, D_{\mathrm{I}}' = 0, \tag{32a}$$

$$K_{\mathrm{Ds}}^{l} = \lim_{l \to -c^l} \sqrt{2\pi(l + c^l)}\, D_{\mathrm{I}}' = 0. \tag{32b}$$

We assume that there are $N_3^{l(1)}$ and $N_3^{r(1)}$ elements on the left- and right-hand sides of the electric yielding zones. Then, by using the solution derived in previous subsection, we can obtain a numerical solution of the problem. Based on the solution, we can calculate the electric displacement intensity factor $K_{\mathrm{Ds}}^{r}(N_3^{r(1)})$ at $l=c_r$ and $K_{\mathrm{Ds}}^{l}(N_3^{l(1)})$ at $l=-c_l$. If $K_{\mathrm{Ds}}^{r}(N_3^{r(1)})>0$, one element is added to the right end of the electric yielding zone, and a new value of N_3^r is obtained, $N_3^{r(2)}=N_3^{r(1)}+1$. On the other hand, if $K_{\mathrm{Ds}}^{r}(N_3^{r(1)})<0$, one element is removed from the right end of the electric yielding zone, and $N_3^{r(2)}=N_3^{r(1)}-1$; The same iterative method is used for the left-hand side electric zone. This process is applied iteratively until the solution satisfies

$$\begin{aligned} &K_{\mathrm{Ds}}^{r}\left(N_3^{r(n_1-1)}\right)\cdot K_{\mathrm{Ds}}^{r}\left(N_3^{r(n_1)}\right) < 0, \\ &K_{\mathrm{Ds}}^{l}\left(N_3^{l(n_2-1)}\right)\cdot K_{\mathrm{Ds}}^{l}\left(N_3^{l(n_2)}\right) < 0, \end{aligned} \tag{33}$$

where n_1 and n_2 are the number of iterations in the yielding zones. Finally, one obtains the sizes of the yielding zones,

$$N_3^r = N_3^{r(n_1)} - 1, \quad R^r = \frac{c^r - c}{c} = \left(N_3^r + \frac{K_{\mathrm{Ds}}^{r}\left(N_3^r\right)}{K_{\mathrm{Ds}}^{r}\left(N_3^r\right) - K_{\mathrm{Ds}}^{r}\left(N_3^r+1\right)}\right)\frac{d}{c}, \tag{34a}$$

$$N_3^l = N_3^{l(n_2)} - 1, \quad R^l = \frac{c^l - c}{c} = \left(N_3^l + \frac{K_{\mathrm{Ds}}^{l}\left(N_3^l\right)}{K_{\mathrm{Ds}}^{l}\left(N_3^l\right) - K_{\mathrm{Ds}}^{l}\left(N_3^l+1\right)}\right)\frac{d}{c}, \tag{34b}$$

where d is the half length of one element in the yielding zone.

7 Numerical solutions

As numerical examples, we assume that there is a crack with arbitrary angle β to the y-axis, centered at the origin of the coordinate system, as schematically shown in Fig. 1. The crack is further within a rectangular piezoelectric plate of PZT-5H with the poling direction along z-axis. The problem is analyzed by using the proposed NLHDD-FS method. Only the mechanical load p and electrical load ω are applied. The details on selecting the collocation and source points and the corresponding convergence issue in the NLHDD-FS method are described in [18,19]. In this example, the element numbers are $N_1=200$, $N_2=100$, and N_3 is determined by the electric yielding zone.

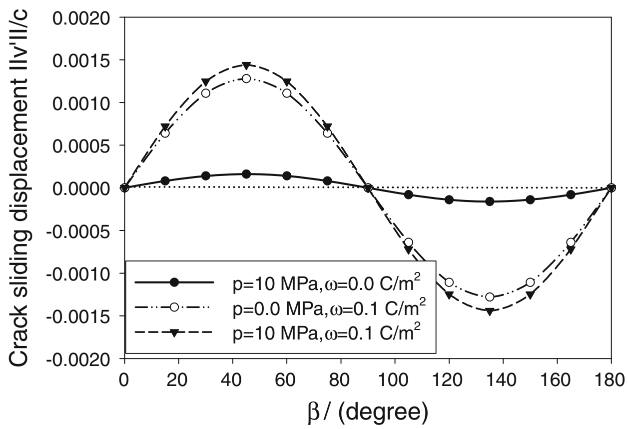

Fig. 2 The crack sliding displacement $\|v'\|$ at the middle point of the crack versus the crack orientation β in an infinite piezoelectric medium

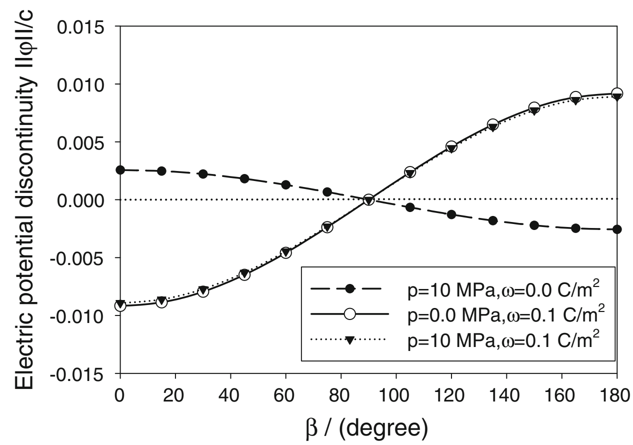

Fig. 4 Electric potential jump $\|\varphi\|$ at the middle point of the crack versus the crack orientation β in an infinite piezoelectric medium

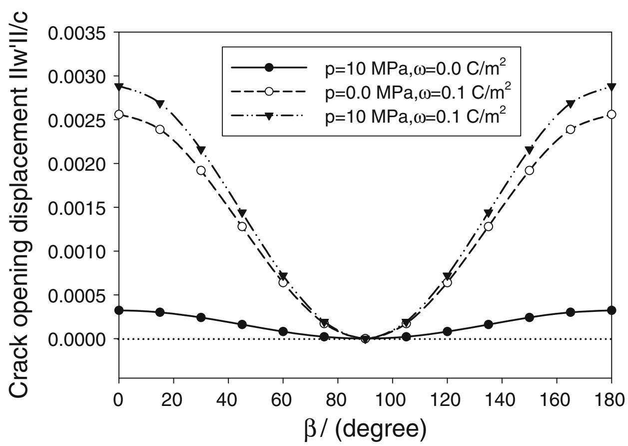

Fig. 3 Crack opening displacement $\|w'\|$ at the middle point of the crack versus the crack orientation β in an infinite piezoelectric medium

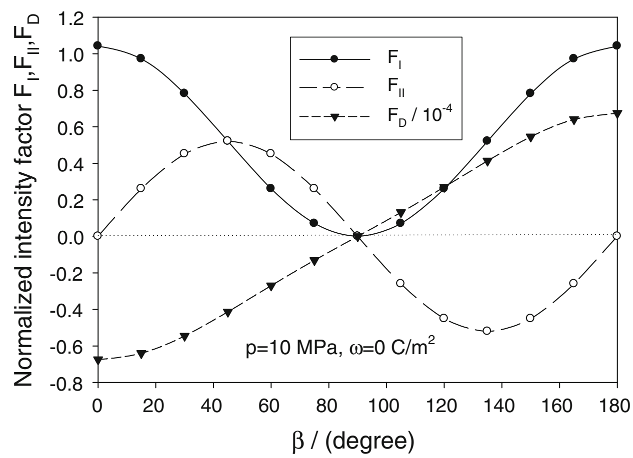

Fig. 5 Normalized extended intensity factors versus crack orientation β under $p = 10\,\text{MPa}$, $\omega = 0\,\text{C/m}^2$ in an infinite piezoelectric medium

7.1 Effect of the crack orientation on the elastic fracture

We first analyze a crack in an infinite plane. To simulate the infinite plane, we selected a very large plate with $a/c = 100$ and $b/a = 4$ as in Fan et al. [18]. Under different mechanical and electric loadings, Figures 2, 3 and 4 show the crack sliding displacement $\|v'\|$, the crack opening displacement $\|w'\|$ and the potential jump $\|\varphi\|$ at the middle point of the crack versus the crack orientation β, where

$$\|v'\| = \|v\|\cos\beta + \|w\|\sin\beta, \tag{35a}$$

$$\|w'\| = -\|v\|\sin\beta + \|w\|\cos\beta. \tag{35b}$$

It can be seen that when $\beta = 0°$, the crack sliding displacement equals to zero and the crack opening displacement reaches a maximum. The crack sliding displacement increases gradually and reaches its maximum at $\beta = 45°$, whilst the crack opening displacement decreases with increasing angle β. Furthermore, the crack sliding displacement and potential jump are anti-symmetric about $\beta = 90°$ whilst the crack opening displacement is symmetric.

The extended intensity factors under different loadings are shown in Figs. 5, 6, 7. Figure 5 shows the normalized extended intensity factors versus the crack orientation β under pure mechanical load

$$p = 10\,\text{MPa}, \quad \omega = 0\,\text{C/m}^2, \tag{36}$$

where the normalized extended intensity factors F_{I}, F_{II} and F_{D} are defined by

$$F_{\mathrm{I}} = \frac{K_{\mathrm{I}}}{p\sqrt{\pi c}}, \quad F_{\mathrm{II}} = \frac{K_{\mathrm{II}}}{p\sqrt{\pi c}}, \quad F_{\mathrm{D}} = \frac{K_{\mathrm{D}}}{\chi p\sqrt{\pi c}}, \tag{37}$$

where

$$\chi = K_{33}/e_{33}. \tag{38}$$

The crack sliding displacement leads to an intensity factor F_{II} which reaches its maximum value at $\beta = 45°$. The results also demonstrate that the intensity factor F_{I} is symmetric,

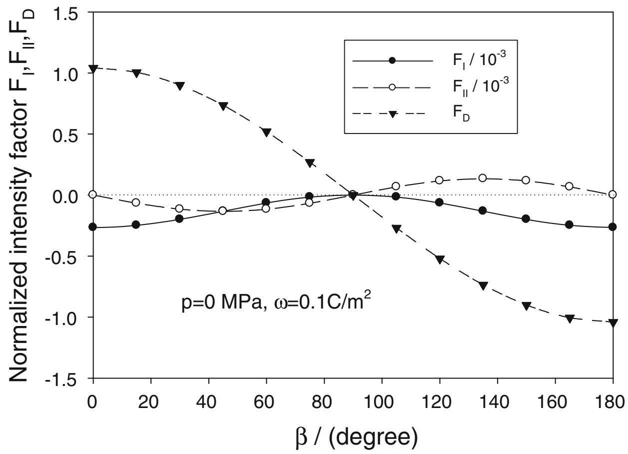

Fig. 6 Normalized extended intensity factors versus crack orientation β under $p = 0\,\text{MPa}, \omega = 0.1\,\text{C/m}^2$ in an infinite piezoelectric medium

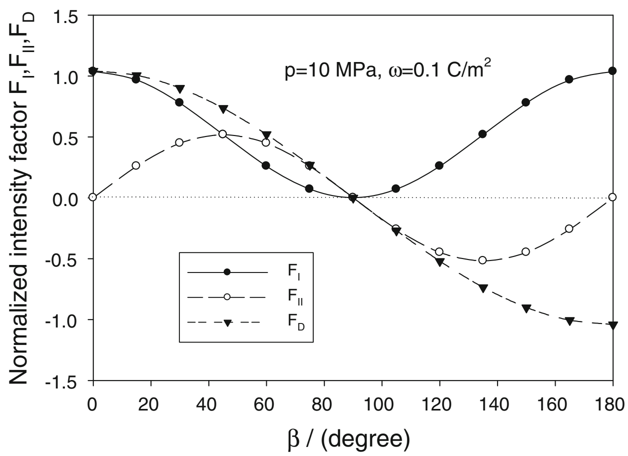

Fig. 7 Normalized extended intensity factors versus crack orientation β under $p = 10\,\text{MPa}, \omega = 0.1\,\text{C/m}^2$ in an infinite piezoelectric medium

while the intensity factors F_{II} and F_{D} are anti-symmetric about $\beta = 90°$. The intensity factor F_{D} is very close to zero under pure mechanical load.

Figure 6 shows the normalized extended intensity factors versus the crack orientation β under pure electric load

$$p = 0\,\text{MPa}, \quad \omega = 0.1\,\text{C/m}^2, \tag{39}$$

where the normalized extended intensity factors F_{I}, F_{II} and F_{D} are defined by

$$F_{\text{I}} = \frac{\chi K_{\text{I}}}{\omega\sqrt{\pi c}}, \quad F_{\text{II}} = \frac{\chi K_{\text{II}}}{\omega\sqrt{\pi c}}, \quad F_{\text{D}} = \frac{K_{\text{D}}}{\omega\sqrt{\pi c}}. \tag{40}$$

It can be seen that the intensity factor F_{D} decreases with increasing β and is further anti-symmetric about $\beta = 90°$. It is also interesting to observe that the stress intensity factors F_{I} and F_{II} are both small under pure electric load, with F_{I} being symmetric and F_{II} anti-symmetric about $\beta = 90°$. It is further noted that F_{I} is negative even though the crack

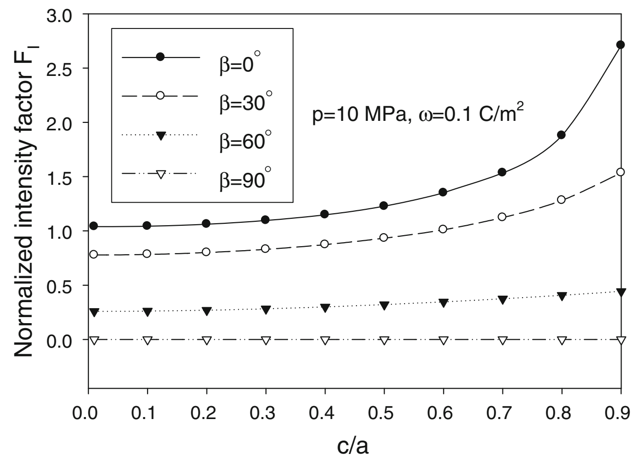

Fig. 8 Normalized stress intensity factor F_{I} versus crack length for different crack orientations under fixed loadings $p = 10\,\text{MPa}, \omega = 0.1\,\text{C/m}^2$ in a finite piezoelectric medium

opening displacement $\|w'\|$ is positive, i.e., the crack is still opening. This striking feature is due to the inverse piezoelectric effect.

Figure 7 shows the normalized extended intensity factors versus the crack orientation β under both electric and mechanical loads

$$p = 10\,\text{MPa}, \quad \omega = 0.1\,\text{C/m}^2, \tag{41}$$

where the normalized extended intensity factors F_{I}, F_{II} and F_{D} are defined by

$$F_{\text{I}} = \frac{K_{\text{I}}}{p\sqrt{\pi c}}, \quad F_{\text{II}} = \frac{K_{\text{II}}}{p\sqrt{\pi c}}, \quad F_{\text{D}} = \frac{K_{\text{D}}}{\omega\sqrt{\pi c}}. \tag{42}$$

Under this combined loading, the extended intensity factors F_{I}, F_{II} and F_{D} show clearly the coupling effect where both the mechanical and electric intensity factors have the same magnitude, while still keeping their symmetric (F_{I}) and anti-symmetric (F_{II} and F_{D}) features about $\beta = 90°$. Therefore, in the following examples, we concentrate on the combined mechanical-electric loading case.

The normalized extended intensity factors versus the normalized crack length for the inclined crack are plotted in Figs. 8, 9, 10. It is shown that, for a given crack orientation, the extended intensity factors F_{I}, F_{II} and F_{D} all increase with increasing crack length, except for F_{II} (Fig. 9) where it is zero when the crack is horizontal ($\beta = 0°$) or vertical ($\beta = 90°$).

7.2 Effect of crack orientation on elastic–plastic fracture

Figure 11 shows the dependence of the electric displacement intensity factor K_{Ds} on R, the parameter related to the electric yielding zone (or equivalently the number of elements in the electric yielding zone). For the case studied here, the size of the electric yielding zone on the right-hand side of the

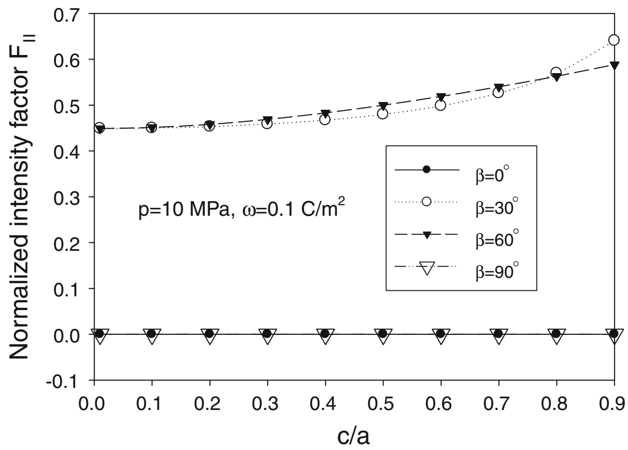

Fig. 9 Normalized stress intensity factor F_{II} versus crack length for different crack orientations under fixed loadings $p = 10\,\text{MPa}, \omega = 0.1\,\text{C/m}^2$ in a finite piezoelectric medium

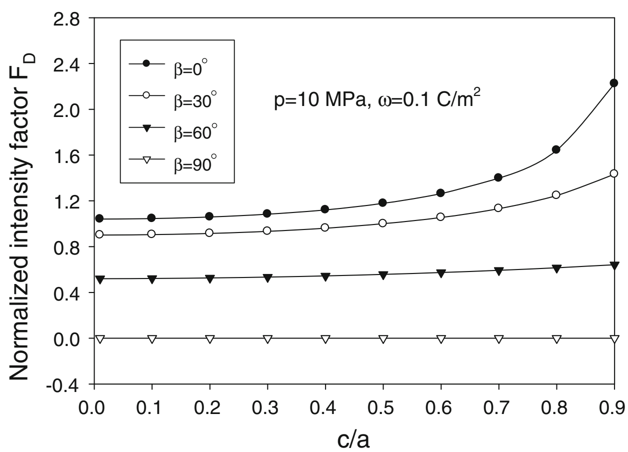

Fig. 10 Normalized electric displacement intensity factor F_D versus crack length for different crack orientations under fixed loadings $p = 10\,\text{MPa}, \omega = 0.1\,\text{C/m}^2$ in a finite piezoelectric medium

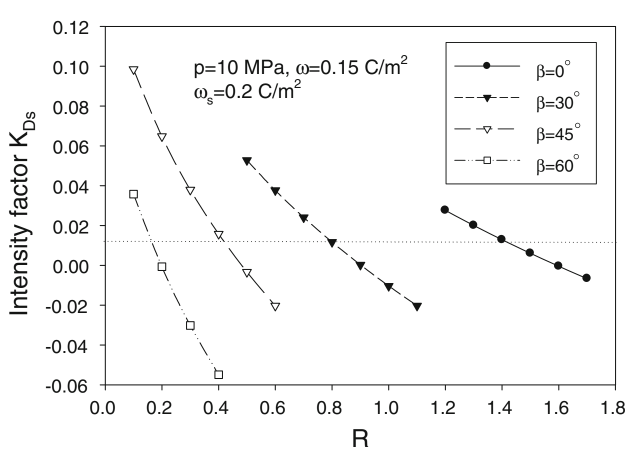

Fig. 11 Electric displacement intensity factor K_{Ds} versus R, a parameter related to the electric yielding zone in PS model. Only $K_{\text{Ds}} = 0$ corresponds to the real size of the electric yielding zone in an infinite piezoelectric medium

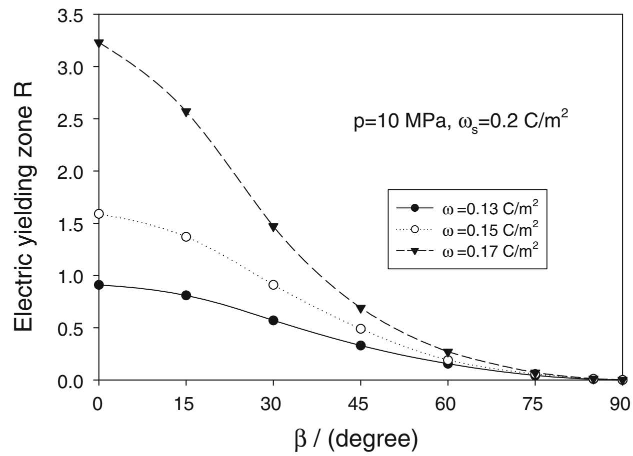

Fig. 12 Electric yielding zone versus crack orientation β under different electric loadings in an infinite piezoelectric medium

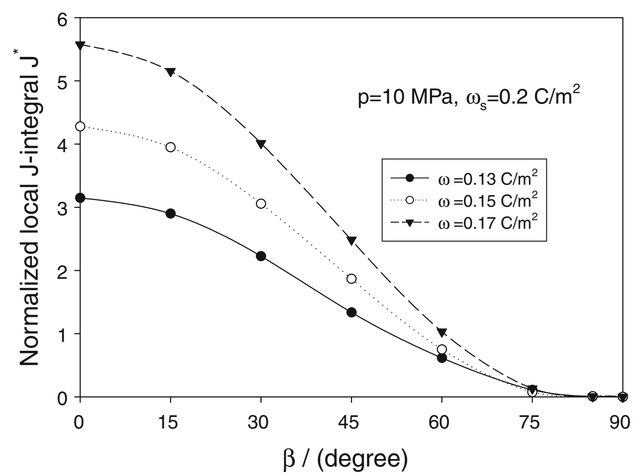

Fig. 13 Normalized local J-integral versus crack orientation β under different electric loadings in an infinite piezoelectric medium

crack tip is equivalent to that on the left-hand side, namely $R = R_{\text{e}}^r = R_{\text{e}}^l$, $N_3 = \frac{1}{2}N_3^r = \frac{1}{2}N_3^l$. It should be pointed out that only the special value of R for which $K_{\text{Ds}} = 0$ gives real size of the electric yielding zone (as given in Eq. (32)).

Figures 12 and 13 show the real size (or length) of the electric yielding zone R (where $K_{\text{Ds}} = 0$) and the local J-integral, respectively, versus the crack orientation under the combined mechanical/electric loads with fixed $p = 10$ MPa but varying ω. The electric displacement saturation is fixed at $\omega_{\text{s}} = 0.1\,\text{C/m}^2$ and the local J-integral is normalized by

$$J^* = \frac{c_0 J^{(l)}}{cp^2}, \tag{43}$$

with $c_0 = 1.0\,\text{GPa}$ being the apparent elastic constant. The length of the electric yielding zone and the local J-integral all decrease with increasing crack angle β. The larger the electric loading is, the longer the electric yielding zone is (Fig. 12).

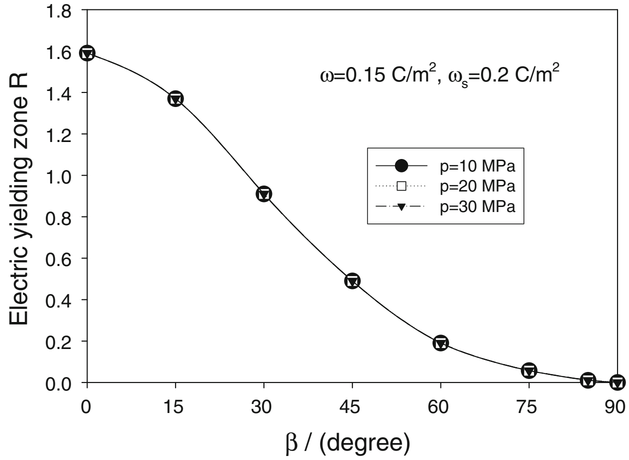

Fig. 14 Electric yielding zone versus crack orientation β under different mechanical loadings in an infinite piezoelectric medium

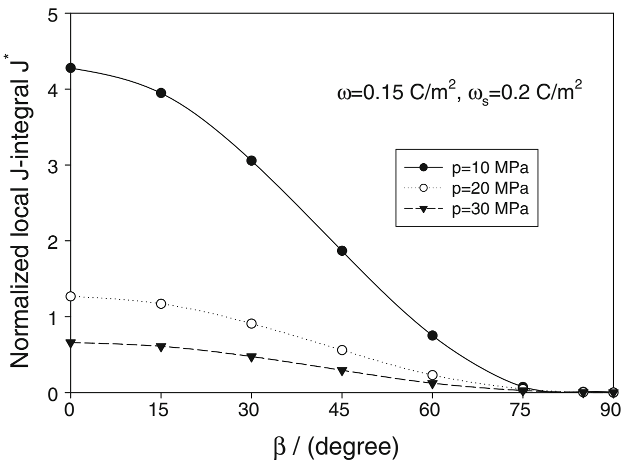

Fig. 15 Normalized local J-integral versus crack orientation β under different mechanical loadings in an infinite piezoelectric medium

The local J-integral shows also a similar trend with respect to the crack orientation (Fig. 13). Also one can observe clearly from these two figures that when $\beta = 90°$, the length of the electric yielding zone and the local J-integral are both become zero.

Under different mechanical loadings, the sizes of the electric yielding zone and the local J-integral versus the crack orientation are displayed respectively in Figs. 14 and 15 for the crack in an infinite piezoelectric plane. It is observed that, for a fixed crack orientation, the local J-integral decreases with increasing mechanical loading (Fig. 15) whilst the influence of the mechanical loading on the electric yielding is very small (Fig. 14) and can thus be ignored. The latter feature is consistent with the analytical solution in Gao et al. [11].

Figures 16 and 17 plot, respectively, the size of the electric yielding zone and the local J-integral versus the crack length in a finite piezoelectric strip with different crack orientations and mechanical loadings. These results demonstrate that both

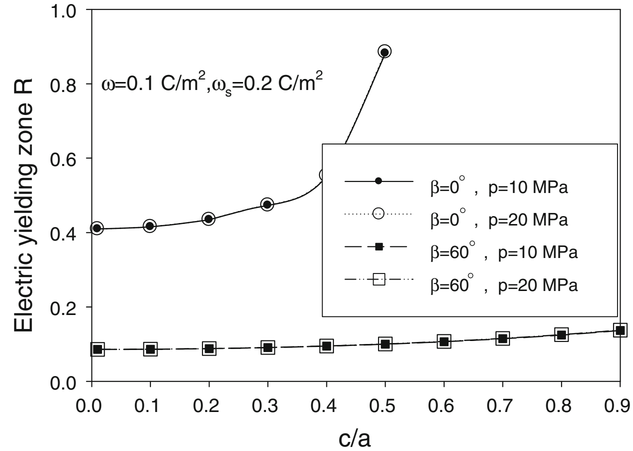

Fig. 16 Electric yielding zone versus crack length with different crack orientations and different mechanical loadings in a finite piezoelectric medium

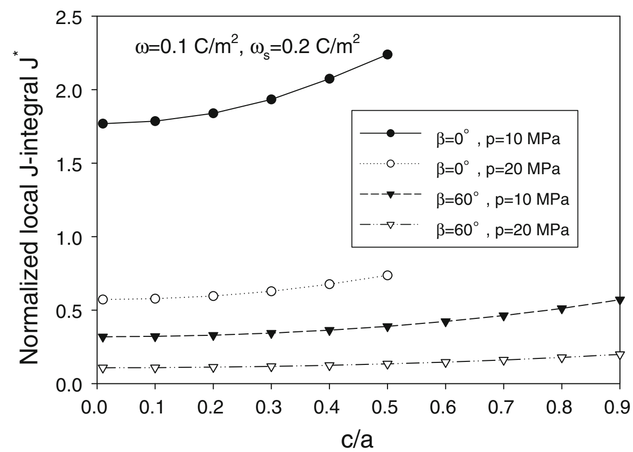

Fig. 17 Normalized local J-integral versus crack length with different crack orientations and different mechanical loading in a finite piezoelectric medium

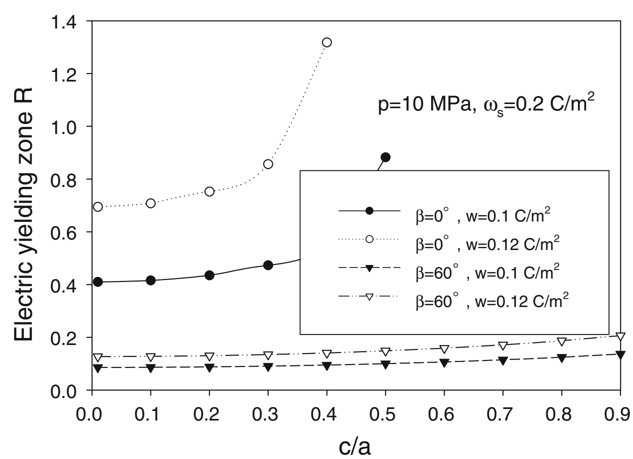

Fig. 18 Electric yielding zone versus crack length with different crack orientations and different electric loadings in a finite piezoelectric medium

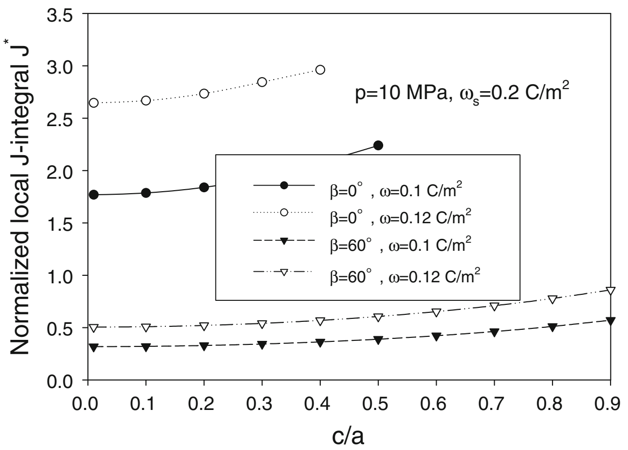

Fig. 19 Normalized local J-integral versus crack length with different crack orientations and different electric loadings in a finite piezoelectric medium

the geometric size and crack orientation can greatly affect the electric yielding zone and the local J-integral, especially when the crack angle is small. Under different electric loadings, Figures 18 and 19 display respectively the size of the electric yielding zone and the local J-integral versus crack length for different crack orientations. Similar to the different mechanical loading case, the size of the electric yielding zone and the local J-integral are more sensitive to the crack length when the crack angle is small.

8 Concluding remarks

The conventional displacement discontinuity method has been extended to analyze arbitrarily oriented electrically nonlinear crack in a finite 2D piezoelectric medium. By using the derived extended Green's functions corresponding to the extended point displacement discontinuities of an arbitrarily oriented crack, the extended field intensity factors near the crack tip are expressed in terms of the extended displacement discontinuity on crack faces. The NLHEDD-FS method combined with an iterative approach has been used to study the nonlinear fracture behavior in finite and infinite piezoelectric media. Numerical results demonstrate that the proposed method is efficient for the examples presented and that both the finite size of the problem domain and the crack orientation could significantly influence the fracture features of the inclined crack.

We point out that while the present analysis is for a homogeneous medium, it can be extended to the corresponding bimaterial system to study the influence of piezoelectric material mismatch or free surface on crack behaviors [24,25].

Acknowledgments The work was supported by the National Natural Science Foundation of China (No. 11102186, No. 11072221, No. 11172273), the Program for Innovative Research Team (in Science and Technology) in University of Henan Province (2010IRTSTHN013), and the Bairen Program in Henan Province.

Appendix A

The material related constants in Eq. (12) are given by

$$\begin{aligned}
L^i_{fyy21} &= \omega_{i1}\,[-c_{11}D_i + s_i(c_{13}A_i - e_{31}B_i)]\,,\\
L^i_{fyy22} &= (c_{11} - c_{12} - \xi_i)\,[c_{11}D_i - s_i(c_{13}A_i - e_{31}B_i)]\,,\\
L^i_{fyy31} &= \omega_{i1}\,[c_{11}D_i - s_i(c_{13}A_i - e_{31}B_i)]\,,\\
L^i_{fyy32} &= \theta_{i1}\,[c_{11}D_i - s_i(c_{13}A_i - e_{31}B_i)]\,,\\
L^i_{fyy41} &= \omega_{i2}\,[c_{11}D_i - s_i(c_{13}A_i - e_{31}B_i)]\,,\\
L^i_{fyy42} &= \theta_{i2}\,[c_{11}D_i - s_i(c_{13}A_i - e_{31}B_i)]\,,
\end{aligned}\tag{A1}$$

$$\begin{aligned}
L^i_{fy21} &= (c_{11} - c_{12} - \xi_i)\,[c_{44}D_is_i + c_{44}A_i - e_{15}B_i]\,,\\
L^i_{fy22} &= \omega_{i1}\,[c_{44}D_is_i + c_{44}A_i - e_{15}B_i]\,,\\
L^i_{fy31} &= \theta_{i1}\,[c_{44}D_is_i + c_{44}A_i - e_{15}B_i]\,,\\
L^i_{fy32} &= \omega_{i1}\,[-c_{44}D_is_i - c_{44}A_i + e_{15}B_i]\,,\\
L^i_{fy41} &= \theta_{i2}\,[c_{44}D_is_i + c_{44}A_i - e_{15}B_i]\,,\\
L^i_{fy42} &= \omega_{i2}\,[-c_{44}D_is_i - c_{44}A_i + e_{15}B_i]\,,
\end{aligned}\tag{A2}$$

$$\begin{aligned}
L^i_{f21} &= \omega_{i1}\,[-c_{13}D_i + s_i(c_{33}A_i - e_{33}B_i)]\,,\\
L^i_{f22} &= (c_{11} - c_{12} - \xi_i)\,[c_{13}D_i - s_i(c_{33}A_i - e_{33}B_i)]\,,\\
L^i_{f31} &= \omega_{i1}\,[c_{13}D_i - s_i(c_{33}A_i - e_{33}B_i)]\,,\\
L^i_{f32} &= \theta_{i1}\,[c_{13}D_i - s_i(c_{33}A_i - e_{33}B_i)]\,,\\
L^i_{f41} &= \omega_{i2}\,[c_{13}D_i - s_i(c_{33}A_i - e_{33}B_i)]\,,\\
L^i_{f42} &= \theta_{i2}\,[c_{13}D_i - s_i(c_{33}A_i - e_{33}B_i)]\,,
\end{aligned}\tag{A3}$$

$$\begin{aligned}
L^i_{dy21} &= (c_{11} - c_{12} - \xi_i)\,[e_{15}D_is_i + e_{15}A_i + K_{11}B_i]\,,\\
L^i_{dy22} &= \omega_{i1}\,[e_{15}D_is_i + e_{15}A_i + K_{11}B_i]\,,\\
L^i_{dy31} &= \theta_{i1}\,[e_{15}D_is_i + e_{15}A_i + K_{11}B_i]\,,\\
L^i_{dy32} &= \omega_{i1}\,[-e_{15}D_is_i - e_{15}A_i - K_{11}B_i]\,,\\
L^i_{dy41} &= \theta_{i2}\,[e_{15}D_is_i + e_{15}A_i + K_{11}B_i]\,,\\
L^i_{dy42} &= \omega_{i2}\,[-e_{15}D_is_i - e_{15}A_i - K_{11}B_i]\,,
\end{aligned}\tag{A4}$$

$$\begin{aligned}
L^i_{d21} &= \omega_{i1}\,[-e_{31}D_i + s_i(e_{33}A_i + K_{33}B_i)]\,,\\
L^i_{d22} &= (c_{11} - c_{12} - \xi_i)\,[e_{13}D_i - s_i(e_{33}A_i + K_{33}B_i)]\,,\\
L^i_{d32} &= \theta_{i1}\,[e_{31}D_i - s_i(e_{33}A_i + K_{33}B_i)]\,,\\
L^i_{d31} &= \omega_{i1}\,[e_{31}D_i - s_i(e_{33}A_i + K_{33}B_i)]\,,\\
L^i_{d42} &= \theta_{i2}\,[e_{31}D_i - s_i(e_{33}A_i + K_{33}B_i)]\,,\\
L^i_{d41} &= \omega_{i2}\,[e_{31}D_i - s_i(e_{33}A_i + K_{33}B_i)]\,.
\end{aligned}\tag{A5}$$

References

1. Suo Z, Kuo CM, Barnett DM, Willis JR (1992) Fracture mechanics for piezoelectric ceramics. J Mech Phys Solids 40:739–765
2. Pan E (1999) A BEM analysis of fracture mechanics in 2D anisotropic piezoelectric solids. Eng Anal Bound Elem 23:67–76
3. Zhang TY, Zhao MH, Tong P (2002) Fracture of piezoelectric ceramics. Adv Appl Mech 38:147–289
4. Kuna M (2010) Fracture mechanics of piezoelectric materials—where are we right now?. Eng Fract Mech 77:309–326
5. Erdogan F, Aksogan O (1974) Bonded half planes containing an arbitrarily oriented crack. Int J Solids Struct 10:569–585
6. Erdogan F, Arin K (1975) A half plane and a strip with an arbitrarily located crack. Int J Fract 11:191–204
7. Tian WY, Chau KT (2003) Arbitrarily oriented crack near interface in piezoelectric bimaterials. Int J Solids Struct 40:1943–1958
8. Wang XD, Jiang LY, Alberta E (2004) The nonlinear fracture behavior of an arbitrarily oriented dielectric crack in piezoelectric materials. Acta Mech 172:195–210
9. Chue CH, Weng SM (2005) Fracture analysis of piezoelectric materials with an arbitrarily oriented crack using energy density theory. Comput Struct 83:1251–1265
10. Ang WT, Athanasius L (2011) Dynamic interaction of multiple arbitrarily oriented planar cracks in a piezoelectric space: a semi-analytic solution. Eur J Mech A 30:608–618
11. Gao H, Zhang TY, Tong P (1997) Local and global energy release rates for an electrically yielded crack in a piezoelectric ceramic. J Mech Phys Solids 45:491–510
12. Dugdale DS (1960) Yielding of steel sheets containing slits. J Mech Phys Solids 8:100–104
13. Zhang TY, Zhao MH, Cao CF (2005) The strip dielectric breakdown model. Int J Fract 132:311–327
14. Ru CQ, Mao X (1999) Conducting crack in a piezoelectric ceramics of limited electrical polarization. J Mech Phys Solids 47:2125–2146
15. Beom HG, Kim YH, Cho C, Kim CB (2006) Asymptotic analysis of an impermeable crack in an electrostrictive material subjected to electric loading. Int J Solids Struct 43:6869–6886
16. Gao CF, Noda N, Zhang TY (2006) Dielectric breakdown model for a conductive crack and electrode in piezoelectric materials. Int J Eng Sci 44:256–272
17. Loboda V, Lapusta Y, Sheveleva A (2010) Limited permeable crack in an interlayer between piezoelectric materials with different zones of electric saturation and mechanical yielding. Int J Solids Struct 47:1796–1806
18. Fan CY, Zhao MH, Zhou YH (2009) Numerical solution of polarization saturation/dielectric breakdown model in 2D finite piezoelectric media. J Mech Phys Solids 57:1527–1544
19. Zhao MH, Xu GT, Fan CY (2009) Hybrid extended displacement discontinuity-charge simulation method for analysis of cracks in 2D piezoelectric media. Eng Anal Bound Elem 33:592–600
20. Zhao MH, Xu GT, Fan CY (2010) Numerical method of crack analysis in 2D finite magnetoelectroelastic media. Comput Mech 45:401–413
21. Fan CY, Zhao MH (2011) Nonlinear fracture of 2D magnetoelectroelastic media: analytical and numerical solutions. Int J Solids Struct 48:2373–2382
22. Ding HJ, Chen WQ, Jiang AM (2004) Green's functions and boundary element method for transversely isotropic piezoelectric materials. Eng Anal Bound Elem 8:975–987
23. Zhao MH, Fan CY, Liu T, Yang F (2007) Extended displacement discontinuity Green's functions for three dimensional transversely isotropic magneto-electro-elastic media and applications. Eng Anal Bound Elem 31:547–558
24. Qin QH, Yu SW (1997) An arbitrarily-oriented plane crack terminating at interface between dissimilar piezoelectric materials. Int J Solids Struct 34:581–590
25. Qin QH, Mai YW (1997) Crack growth prediction of an inclined crack in a half-plane thermopiezoelectric solid. Theor Appl Fract Mech 26:185–191